

## Photoelectron Spectroscopy

READING: Cheetham and Day, Volume 1, Chapter 3, pp. 84-121.

F.A. Stevie, C.L. Donley, "Introduction to X-ray Photoelectron Spectroscopy,"  
*J. Vac. Sci. Technol.* **2020**, *A38*, 063204 ([link](#))

G. Greczynski, L. Hultman, "A Step-by-Step Guide to Perform X-ray Photoelectron Spectroscopy," *J. Appl. Phys.* **2022**, *132*, 011101 ([link](#))

P. van der Heide, "X-ray Photoelectron Spectroscopy," John Wiley & Sons, Inc., Hoboken, NJ, USA: 2012.

**(41)** *Photoelectron spectroscopy* (PES) is an important characterization tool for solid-state scientists. It is based on the "simple" idea that electromagnetic radiation of sufficient energy impinging on a metal can eject electrons from the metal. Einstein used this experiment to establish the particle nature of light. There are two regimes of the PES experiment depending on the energies of the incident photons: (i) X-ray photoelectron spectroscopy (XPS) gives information about core and valence electrons and their states; and (ii) ultraviolet photoelectron spectroscopy (UPS) gives information about just valence electrons and their states. The experiment is most reliable for metallic substances, but it can be carried out on nonmetallic solids. K. Siegbahn developed PES for chemical analysis (ESCA = electron spectroscopy for chemical analysis) and won the 1981 Nobel Prize in Physics for this development. However, it is fundamentally a *surface* technique and cannot provide completely reliable analytical data for bulk samples.

Alternative methods include electron microprobe analysis (EMPA), scanning electron microscopy (SEM), and inductively-coupled plasma/mass spectrometry (ICP-MS). Each of these methods offers its own strengths and weaknesses. Furthermore, EMPA and SEM provide similar outcomes although SEM instrumentation is designed for materials imaging. For best overall results, a combination of analytical techniques is needed to properly characterize a solid sample. If the sample is polycrystalline, you can use X-ray powder diffraction to provide a chemical analysis, but again you need to take care for the limitations of the method. For example, if the crystal contains two elements differing by one atomic number, e.g., Fe and Co, you will not be able to distinguish the two elements and obtain an unequivocal determination of composition.

**(42)** *Background:* The foundation of PES is the removal of an electron from an atom in a metal when light of sufficient energy interacts with the metal. For any metal, the highest occupied level is called the *Fermi level*  $E_F$  and the valence electrons occupy a quasi-continuous conduction band extending below  $E_F$ . At much deeper energy values are the core electron states. To release a photoelectron, the energy of an incident photon must exceed the *binding energy* of the electron  $E_B$ . Then, by energy conservation, any excess energy goes toward kinetic energy of the released photoelectron:

$$h\nu = E_B(e^-) + E_{KE}(e^-).$$

Incident photons typically have fixed energy depending on the source. For XPS, X-rays will have energies 200-2000 eV; for UPS, vacuum ultra-violet radiation with energies 10-45 eV are used. To eject a photoelectron there is a minimum photon energy needed, which is based on the work function ( $\phi$ ) for the material,  $h\nu_{\min} = e\phi$ , and are typically 2-6 eV. This amount of energy is needed to take an electron from the Fermi level and release it from the solid to the vacuum. In general, the work function is not a characteristic of the bulk material, but it depends on the surface properties of the solid. For example,  $\phi(\text{Au})$  depends on the indices of the surface planes:

$\phi_{100}(\text{Au}) = 5.47 \text{ eV}$ ;  $\phi_{110}(\text{Au}) = 5.37 \text{ eV}$ ;  $\phi_{111}(\text{Au}) = 5.31 \text{ eV}$ . Perhaps more importantly, the ejected photoelectrons enter a spectrometer, which has its own characteristic work function. Since the sample and spectrometer are in “electronic equilibrium,” it is important to include a standard that provides a reference for proper binding energy determinations.

Therefore, incident photons with frequencies  $\nu > \nu_{\text{min}}$  are needed and photoelectrons can emerge for all occupied states of the substance with binding energy less than the photon energy. As a result, the maximum kinetic energy of photoelectrons are observed for electrons ejected at the Fermi level:  $E_{\text{KE}}^{\text{max}} = h\nu - e\phi$ .

**(43)** Each element has characteristic core electron binding energies, the concept that motivated K. Siegbahn to develop PES for chemical analysis (ESCA). As we proceed along the periodic table of the elements, the binding energies of electrons steadily increase. Therefore, depending on the incident photon energy, only certain electrons can be ejected as photoelectrons. For example, XPS measurements of the element Sn ( $Z = 50$ ) can only provide information on the following atomic orbitals:  $3s, 3p, 3d$ ;  $4s, 4p, 4d$ ;  $5s, 5p$ ; UPS measurements are limited to  $5s, 5p$  and possibly  $4d$ . The important outcomes of any PES experiment include (i) chemical shifts, which correspond to the binding energies associated with the various occupied electronic states; (ii) multiplet structures arising primarily from spin-orbit splitting, which will occur for electrons ejected from  $p, d, f, \dots$  levels; and (iii) satellite peaks, which depend on the incident radiation.

**(44)** *The PES Experiment:* The nature of a PES experiment involves four essential components:

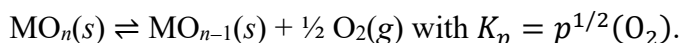
- *Radiation Sources:* Synchrotron radiation allows continuously tunable frequencies for X-rays, but demands a large site. Manageable spectrometers utilize Mg or Al  $K\alpha$  radiation to optimize photoelectron flux and resolution. Mg  $K\alpha$  is 1.254 keV; Al  $K\alpha$  is 1.487 keV. Al  $K\alpha$  radiation allows  $\sim 0.9 \text{ eV}$  resolution after taking into account spin-orbit splitting and the lifetime of the hole state. At the expense of incident intensity and photoelectron flux, the X-radiation can be focused by Bragg diffraction. UPS utilizes either He(I) or He(II) radiation at 21.21 eV and 40.8 eV, respectively. These emissions give better resolution than XPS, a smaller overall energy window for measurements, and distorted backgrounds at high binding energies.
- *Spectrometer:* For XPS, the detector of choice utilizes deflection of the charged photoelectrons after focusing and before electron multipliers, amplification and computational analysis. Furthermore, ultrahigh vacuum systems with pressures less than  $10^{-9}$  torr are required for reliable and useful outcomes.

**(45)** *The PES Experiment (continued):*

- *Sample Preparation:* Regardless how you plan to use the PES data, a clean sample is imperative. Otherwise, you have no confidence in the quality of the data. XPS provides information about a thin ( $\sim 15 \text{ \AA}$ ) surface layer of the substance. Although X-rays can penetrate to  $\sim 10^3\text{--}10^4 \text{ \AA}$ , the photoelectrons generated in the sample bulk will be inelastically scattered before they reach the surface. The mean free path for photoelectrons generated from 1.487 keV radiation (Al  $K\alpha$ ) lies between 7 and 18  $\text{\AA}$ . Therefore, the sharp, intense peaks in a PE spectrum come from photoelectrons generated near the sample surface. X-rays that penetrate more deeply into the material will eject electrons that are scattered inelastically. These electrons will exhibit lower kinetic energies and, therefore, higher binding energies than if they were released nearer the surface. As a result, PES peaks tend to show broad tails extending toward higher binding energies.

To obtain suitably clean surfaces, solid samples can be cleaved, or Ar-ion sputtering can be used to remove surface impurities or adsorbents. However, there is often some amount of surface oxide or surface carbon, which arises from either reaction with CO<sub>2</sub> to form surface carbonate or from volatile molecules from vacuum grease. The binding energy of the 1s core state of such “adventitious” carbon can provide a useful reference. For nonmetallic samples, gold film can be deposited to provide a metallic surface for an effective experiment.

Fundamentally, however, since the PES experiment is carried out at very low pressures, the substance must be stable in this reduced pressure environment with respect to decomposition products. For example, consider a PES experiment using a metal oxide, MO<sub>n</sub>, which may show a second metal oxide, MO<sub>n-1</sub>. The chemical relationship between these two oxides is



At atmospheric conditions,  $p(\text{O}_2) = 0.2 \text{ atm}$ , MO<sub>n</sub>(s) may be stable relative to the reduced oxide, but in the spectrometer, where  $p(\text{O}_2)$  is much lower, it may not be stable toward decomposition. Therefore, it is very important to know how a substance responds under reduced pressure.

**(46)** *The PES Experiment (continued):*

- *Spectrum Analysis:* The primary outcomes of any photoelectron experiment are the peak positions, peak intensities, and peak shapes, because they provide information about the electronic structure of the material. Peak positions are related to binding energies. They are affected by the position of the reference level, how the spectrometer has been calibrated, whether the material is metallic or nonmetallic, and how the photoelectrons or incident radiation might create phenomena like multiplets, satellites, etc. Intensities are dictated by PE cross-sections, which are energy-dependent probabilities for a PE process to occur. Different atoms show different responses depending on the incident photon energy, and these responses affect the intensity distribution. Ideally, PE spectra close to the Fermi level should reflect the calculated density of states (DOS) curves for the occupied valence states of a solid. However, calculations are carried out on neutral solid. The experiment is affected greatly by the nature of the hole states generated on the atoms ejecting photoelectrons, i.e., M<sup>+</sup> in the MX substance. Spectra are typically plotted as Intensity (counting rate of photoelectrons) vs. Binding energy:

$$E_B = h\nu - E_{KE}.$$

Example: XPS spectrum of Pd(s). Mg K $\alpha$  radiation ( $h\nu = 1.253 \text{ keV}$ ) produces a spectrum with kinetic energies shown between 270 and 1270 eV. There are various peaks with tails evident that occur from energy losses as the photoelectrons leave the solid. The typical spectrum is presented using binding energy ( $E_B = \text{BE} = h\nu - \text{KE}$ ). The most intense peaks come from the core 3s, 3p, 3d electrons; the 3p and 3d peaks show spin-orbit splitting. For example, the 3d orbital ( $l = 2$ ) with one hole ( $s = 1/2$ ) gives peaks associated with  $j = 2 + 1/2 = 5/2$  (3d<sub>5/2</sub>) and  $j = 2 - 1/2 = 3/2$  (3d<sub>3/2</sub>). The degeneracy of each level ( $2j + 1$ ) corresponds to their relative intensities: for 3d<sub>5/2</sub>, the degeneracy is 6; for 3d<sub>3/2</sub>, the degeneracy is 4. Furthermore, the binding energy for 3d<sub>5/2</sub> is lower than that for 3d<sub>3/2</sub>, which means that in the atom, the energy of the 3d<sub>5/2</sub> level is higher than the energy of the 3d<sub>3/2</sub> level.

- (47)** The peak near 920 eV labelled “MNN” is due to an Auger process, which is a 2-electron process: the initial state of the Auger process is the final state for the XPS process. For this specific case, a photoelectron is emitted from the M-shell ( $n = 3$ ). Relaxation follows with an electron

from the  $N$ -shell ( $n = 3$ ) filling the hole created in the  $M$ -shell. During this process, energy is released which allows another  $N$ -shell electron to be emitted; this second electron is an *Auger electron*. Auger spectroscopy is another useful surface analysis technique.

**(48) Chemical Shifts:** From the chemical perspective, the important outcomes of the PES experiment are the binding energies of the photoelectrons.<sup>20</sup> Due to various relaxation processes associated with the final ionized state of an atom in the solid, the measured binding energy of an electron does not equal calculated energy of the core state for the neutral atom. These relaxation processes will typically lower observed binding energies compared to the energy differences between the ground state of the neutral atom and the resulting ionized state via Koopman's theorem. In many cases, an effective " $Z + 1$ " atom is used to interpret the binding energies of core electrons of the final state because the corresponding valence electrons will feel a lower screening of the nucleus and affect the overall potential energy of the atom or ion. The adjustment of the valence electron to the formation of the core-hole gives more kinetic energy to the photoelectron, which leads to a lower binding energy.

Intra-atomic relaxation processes arise largely from single-ion shifts to the valence electron potential energy once a core electron is ejected. Inter-atomic relaxation is the response of the chemical environment to ionization of the atom. The significant environmental response is *polarization*, either of the neighboring ions in insulators and semiconductors or of the conduction electrons in metals. Inter-atomic relaxation tends to counteract the intra-atomic relaxation processes, but generally do not cancel each other.

**(49)** The binding energy of an electron depends on both the formal oxidation state of the element and the local chemical and structural environment of the atom in the solid. Binding energies associated with a given atom generally increase as the oxidation state of that atom increases because electrons feel a stronger attractive coulomb potential from the ion core. This ability to distinguish between different oxidation states and chemical environments is a major asset of XPS. For example, consider metallic  $\text{Ti}(s)$  vs. insulating  $\text{TiO}_2(s)$ . The peaks assigned to Ti  $2p$  orbitals shift by  $\sim 4.6$  eV towards higher binding energy from  $\text{Ti}(s)$  ( $\text{Ti}^0$ ) to  $\text{TiO}_2(s)$  ( $\text{Ti}^{4+}$ ). The spin-orbit splittings into  $2p_{3/2}$  and  $2p_{1/2}$  peaks remain essentially unchanged at  $\sim 6$  eV. The peak shapes are somewhat more symmetrical for  $\text{TiO}_2(s)$  with certain tails toward higher binding energies (lower kinetic energies) for  $\text{Ti}(s)$ . However, using just oxidation state to rationalize chemical shifts can be misleading. For example, there is a negative shift in the  $4f$  binding energies of Pb relative to the Fermi level from insulating  $\text{PbO}(s)$  with  $\text{Pb}^{2+}$  to metallic  $\text{PbO}_2(s)$  with  $\text{Pb}^{4+}$ .<sup>21</sup> In this case, the local environment and corresponding Madelung (ionic) potentials at the Pb sites can influence the observed outcome. In  $\text{PbO}$ , there are four nearest neighbor O atoms and four near neighbor Pb atoms, whereas the rutile-type structure of  $\text{PbO}_2$  involves octahedrally coordinated Pb by O atoms. As a point of speculation, if  $\text{PbO}$  adopted the NaCl-type structure with octahedrally coordinated cations, then we may see the expected shifts in binding energies. Nevertheless, other factors that can affect the peak positions and shapes include build-up of positive charge are the surface, which can create a dipole layer and the exact positions of Fermi levels, which can vary with dopant concentration levels. Resolution of binding energies for atoms exhibiting slightly different chemical shifts is limited by their peak widths, which are primarily affected by the lifetime of the

<sup>20</sup> *Inorg. Chem.* **1984**, 23, 2625-2632.

<sup>21</sup> D.J. Payne, R.G. Egdell, D.S.L. Law, P.-A. Glans, T. Learmonth, K.E. Smith, J. Guo, A. Walsh, G.W. Watson, *J. Mater. Chem.* **2007**, 17, 267-277.

final state, but also depend on the linewidth of the incident radiation and intrinsic variations of the initial state.

**(50)** XPS binding energies can also be used to evaluate changes in the ionic and covalent character of metal-oxygen bonds in complex oxides. Consider a study that compares silica  $\text{SiO}_2(s)$  and zirconia  $\text{ZrO}_2(s)$  with zircon  $\text{ZrSiO}_4(s)$ .<sup>22</sup> In these structures, Si and Zr have +4 formal oxidation states. In silica and zircon, Si atoms are tetrahedrally coordinated by O atoms; in zirconia and zircon, the Zr coordination environments differ: Zr is 7-coordinate in monoclinic  $\text{ZrO}_2$  but it is 8-coordinate in tetragonal zircon. XPS spectra of O 1s, Si 2p, and Zr 3d levels show interesting trends:

- The binding energies of the O 1s peak increase from  $\text{SiO}_2$  to  $\text{ZrSiO}_4$  to  $\text{ZrO}_2$ .
- The binding energies of the Si 2p peak (no spin-orbit coupling observed) increase from  $\text{ZrSiO}_4$  to  $\text{SiO}_2$ .
- The binding energies of the Zr 3d peaks (spin-orbit coupling observed) increase from  $\text{ZrO}_2$  to  $\text{ZrSiO}_4$ .

A simple concept relates the change in binding energies of an elemental component in complex oxides to three components: (i) change in oxidation state of the atom; (ii) change in Madelung potential at the atomic site; and (iii) change in relaxation terms. The authors of this work evaluated changes in the relaxation term by measured binding energies for Auger processes in these materials – they concluded relatively small contributions from relaxation to the observed chemical shifts. According to density-functional electronic structure calculations, the formal negative charge at O atoms increases from  $\text{SiO}_2$  to  $\text{ZrSiO}_4$  to  $\text{ZrO}_2$ ; the formal positive charge at Si atoms decreases from  $\text{SiO}_2$  to  $\text{ZrSiO}_4$ ; and the formal positive charge at Zr atoms decreases from  $\text{ZrSiO}_4$  to  $\text{ZrO}_2$ . The conclusion from the XPS spectra and DFT calculations is that the covalency of the Si–O bonds and the ionicity of the Zr–O bonds increase from their binary oxides to the ternary oxides.

**(51)** *Valence Band Spectra – Metals:* Metallic Au(s) and the intermetallic compound CsAu(s), which is a transparent red insulator.<sup>23</sup> Some features to focus upon include (a) no states at the Fermi level for CsAu, which is indicative of a nonmetals, while the 6s band tails off at the Fermi level in Au; (b) the 5d band in Au is ~7 eV broad, shows satellites to higher binding energy (lower kinetic energy), and possible effects from the broad 6s band as well, whereas the 5d band in CsAu is narrower, which indicates smaller overlap between these orbitals in the solid (Au–Au distances are 2.89 Å in Au and 4.26 Å in CsAu); and (c) there is a positive shift of the binding energy of the valence 5d band as the formal oxidation state of Au decreases from  $\text{Au}^0$  to “ $\text{Au}^{-1}$ ”. This difference could arise from how the Fermi levels are positioned. Nevertheless, the binding energies of the  $4f_{7/2}$  levels are 89.1 eV for Au(s) and 86.8 eV for CsAu(s), an outcome that is consistent with the decrease in oxidation state of Au in the intermetallic compound.

Comparison among Ni(s), Cu(s) and Zn(s). With respect to their corresponding Fermi levels, the 3d peak shifts to increasing binding energy and becomes narrower with increasing effective nuclear charge. The satellite observed in the Ni spectrum arises from 2-electron processes because the incident X-radiation can cause multi-electron transitions within the valence band.

**(52)** *Valence Band Spectra – Oxides:* Comparison of the calculated valence density of states (DOS) curve and the observed valence band XPS spectrum using Mg  $K\alpha$  radiation for  $\text{ReO}_3$ .  $\text{ReO}_3$

<sup>22</sup> M.J. Guittet, J.P. Crocombette, M. Gautier-Soyer, *Phys. Rev. B* **2001**, 63, 125117.

<sup>23</sup> G.K. Westheim, C.W. Bates, Jr., D.N.E. Buchanan, *Solid State Commun.* **1979**, 30, 473-475.

involves a network of vertex-sharing  $[\text{ReO}_6/2]$  octahedra. The calculated DOS graph reveals a small gap that separates Re–O bonding and nonbonding states below from Re–O antibonding states above the gap. Being a  $d^1$  system, a small number of states above this energy gap are occupied in  $\text{ReO}_3$ . Features of the occupied states in the valence DOS curve are evident in the valence band XPS spectrum, but the intensities are different than in the calculation. In the XPS spectrum, states involving significant Re contributions have stronger intensities than other states. For example, a small peak near 4 eV in the XPS spectrum is assigned to O 2p nonbonding states, which form a sharp, distinct peak in the calculated DOS curve. On the other hand, Re–O bonding and antibonding states have more intense peaks in the XPS spectrum. These differences in spectral intensities are due to the different cross-sections for photoelectron emission from Re and O using Mg  $K\alpha$  radiation.

Changes in the XPS valence band spectra for  $\text{VO}_2$  between its metallic and insulating states.  $\text{VO}_2$  changes atomic structure from rutile-type in its metallic state to a monoclinic form with chains of alternating –short-long– V–V distance in its insulating state. The XPS valence band spectrum indicates changes in the density of states at their respective Fermi levels: the peak assigned to the V 3d shows a sharp change at 0 for metallic  $\text{VO}_2$ , but it falls to the baseline for insulating  $\text{VO}_2$ .

**(53)**  $\text{Nb}_3\text{Cl}_8$  and  $\text{Li}_x\text{Nb}_3\text{Cl}_8$ : UPS and XPS provide information about their valence states as well as show significant differences among He(I), He(II), and Mg  $K\alpha$  incident radiation.  $\text{Nb}_3\text{Cl}_8$  has  $\text{Nb}_3$  triangles with 7 valence electrons embedded in close-packed chlorides with point symmetry  $C_{3v}$ . A molecular orbital energy diagram focusing on the  $\text{Nb}_3$  cluster orbitals gives the pattern  $a_1$ - $e$ - $a_1$  of occupied orbitals; the second  $a_1$  molecular orbital is the highest occupied molecular orbitals and is half-filled. Three peaks are clearly observed for binding energies between 0 and 3 eV in the He(II) spectrum and are just observed in the He(I) spectrum. However, the Mg  $K\alpha$  XPS spectrum gives a single broad peak in this region. The peak resolution and relative intensities in the He(II) spectrum between 0-3 eV is clear and agrees with the theoretical calculation that the triangular cluster has three occupied levels. Intercalation of Li disrupts peak shapes in this region and yields a more complex pattern of states in the He(II) spectrum. Whether the clusters distort, or there are mixtures of 7-electron and 8-electron clusters remains to be determined.

**(54)** *Strengths and Limitations of PES:*<sup>24</sup>

Strengths:	Limitations:
Non-destructive, semi-quantitative analysis of materials. Compositions can be determined to within $\pm 10\%$ .	Ultra-high vacuum ( $< 10^{-9}$ torr) is required. Sample stability or volatility can be an issue for successful experiments
Detection of all elements except hydrogen and helium is possible.	Focusing X-ray beams provides large analyzed surface areas, on the order of $\text{mm}^2$ . The signal is an average over many sites.
Small shifts ( $\sim 0.1$ eV) in binding energies can be measured and provide chemical information about the elements in the sample.	Some samples produce severe charging problems, which compromise analysis quality, as photoelectrons are emitted.
Surface contaminants can be removed by Ar ion beam sputtering.	Not appropriate for quantitative bulk analysis; accurate compositions for nanometer-thick layers.

<sup>24</sup> D.Mogk, *X-Ray Photoelectron Spectroscopy*, at [https://serc.carleton.edu/msu\\_nanotech/methods/xps.html](https://serc.carleton.edu/msu_nanotech/methods/xps.html)

(55) Other spectroscopic techniques used for solid-state analysis include:

- Angle-Resolved Photoemission Spectroscopy (ARPES) – probes energies and momenta of electrons in a material by measuring kinetic energies and emission angle distributions of photoelectrons.
- Bremsstrahlung Isochromat Spectroscopy (BIS) – also called Inverse Photoelectron Spectroscopy (IPES); examines the energies of unoccupied states in a material by bombarding a surface with monochromatic electrons, some of which relax into unoccupied states after photoemission.
- Auger Electron Spectroscopy (AES) – characterization technique to examine chemical and compositional surface environments, relying on interstate and intrastate electronic transitions of an excited atom in a material.
- Rutherford Backscattering Spectrometry (RBS) – also called High-Energy Ion Scattering (HEIS); determines material structure and composition by measuring the backscattering of a beam of high energy protons or alpha particles hitting the surface. RBS is especially useful for analyzing heavy element components.
- X-Ray Absorption Spectroscopy (XAS) – determines local geometric and electronic structures of materials. There are three important regions:
  - (i) Absorption Threshold – transitions to lowest unoccupied states
  - (ii) X-ray Absorption Near-Edge Structure (XANES) – formation of many body excited states arising from a core hole after absorption of an X-ray photon. It is element-specific and sensitive to local coordination.
  - (iii) Extended X-ray Absorption Fine Structure (EXAFS) – oscillating regions near absorption edges of XAS spectra; can provide local structural information.
- Electron Energy Loss Spectroscopy (EELS) – analyzes surface composition of thin samples by examining the energy of transmitted electrons; instrumentation is typically incorporated into a transmission electron microscope (TEM).

Other characterization methods for solid-state materials are:

- Various spectroscopies – (near) infra-red (IR / NIR); Raman; and UV-Visible.
- Magnetic resonance – nuclear (NMR; with magic-angle spinning MAS) and electron paramagnetic resonance (EPR).
- Microscopy – optical; scanning electron microscopy (SEM) or electron microprobe (EPMA); transmission electron microscopy (TEM); and scanning probe methods (SPM), such as scanning tunneling (STM) and atomic force (AFM) microscopies.
- Small-angle scattering (SAS) – X-ray (SAXS) or neutron (SANS).
- Thermal characterization – thermal gravimetric analysis (TGA); differential thermal analysis (DTA); and differential scanning calorimetry (DSC).

READING: J.P. Sibilía, *A Guide to Materials Characterization and Chemical Analysis*, 2<sup>nd</sup> Ed., Wiley-VCH, New York, 1996.

K. Sultan, *Practical Guide to Materials Characterization: Techniques and Applications*, Wiley-Online, 2023.